Orbital diamagnetism in multilayer graphenes: Systematic study with the effective mass approximation

Mikito Koshino and Tsuneya Ando
Department of Physics, Tokyo Institute of Technology, 2-12-1 Ookayama, Meguro-ku, Tokyo 152-8551, Japan
(Received 19 April 2007; revised manuscript received 7 June 2007; published 17 August 2007)

We present a theoretical study on the orbital magnetism in multilayer graphenes within the effective mass approximation. The Hamiltonian and thus susceptibility can be decomposed into contributions from subsystems equivalent to monolayer or bilayer graphene. The monolayer-type subband exists only in odd layers and exhibits a delta-function susceptibility at $\varepsilon_F=0$. The bilayer-type subband appearing in every layer number gives a singular structure in the vicinity of $\varepsilon_F=0$ due to the trigonal warping as well as a logarithmic tail away from $\varepsilon_F=0$. The integral of the susceptibility over energy is approximately given only by the layer number.

DOI: 10.1103/PhysRevB.76.085425 PACS number(s): 75.70.−i, 81.05.Uw, 73.22.−f

I. INTRODUCTION

Recently, unconventional electronic properties of monocrystalline graphenes attracts much attention motivated by experimental fabrication,[1–3] although they were already the subject of theoretical study prior to the fabrication.[4–13] Multilayer films which contain more than two layers can also be synthesized, and various phenomena depending on the layer number have been reported.[2,14,15] In this paper, we present a theoretical study on the orbital magnetism in multilayer graphenes.

The electronic structure of the monolayer graphene is quite different from conventional metals because the conduction and valence bands touch at K and K' points in the Brillouin zone, around which the dispersion becomes linear like a relativistic particle. In multilayer graphenes, the interlayer coupling makes a complex structure around the band touching. The electronic properties of graphene bilayer were theoretically studied for the band structure[16,17] and the transport properties.[18–20] For few-layered graphenes of more than two stacks, the electronic structure is investigated theoretically in a $\mathbf{k}\cdot\mathbf{p}$ approximation,[21] a density functional calculation,[22] and a tight-binding model.[23,24] On the experimental side, the band structures of graphenes from one to four layers were recently measured using angle-resolved photoemission spectroscopy.[15]

The orbital magnetism in graphene-based systems was first studied for a monolayer as a simple model to explain the large diamagnetism of graphite.[4] It was found that the susceptibility becomes highly diamagnetic at $\varepsilon=0$ (band touching point) even though the density of states vanishes there. The calculation was extended to graphite[25,26] and to few-layered graphenes as a model of graphite intercalation compounds.[27–29] The Fermi surface of the graphite is known to be trigonally warped around the band touching point[25] and the effect of the warping on magnetization was discussed within the perturbational approach.[26] Recently, the disorder effects on the magnetic oscillation[30,32] and on the susceptibility[31,32] were studied for the monolayer graphene.

Here, we present a systematic study on the orbital magnetism for multilayer graphenes with arbitrary layer numbers in the effective mass approximation. We show that the Hamiltonian of a multilayer graphene can be decomposed into those equivalent to monolayer or bilayer, which allows us to study the dependence of the susceptibility on layer numbers. We take the trigonal warping effect into the calculation and show that the fine structure around zero energy gives rise to singular magnetic properties.

We introduce the model Hamiltonian and its decomposition into subsystems in Sec. II and present the calculation of the magnetization in Sec. III. The discussion and summary are given in Sec. IV.

II. FORMULATION

We consider a multilayer graphene composed of N layers of a carbon hexagonal network, which are arranged in the AB (Bernal) stacking, as shown in Fig. 1. A unit cell contains A_j and B_j atoms on the layer $j=1,\ldots,N$. For convenience, we divide carbon atoms into two groups as

$$\text{Group I: } B_1, A_2, B_3, \ldots, \tag{1}$$

$$\text{Group II: } A_1, B_2, A_3, \ldots, \tag{2}$$

The atoms of group I are arranged along vertical columns normal to the layer plane, while those in group II are above or below the center of hexagons in the neighboring layers. The lattice constant within a layer is given by $a=0.246$ nm and the distance between adjacent layers $c_0/2=0.334$ nm.

The system can be described by a $\mathbf{k}\cdot\mathbf{p}$ Hamiltonian closely related to a three-dimensional (3D) graphite

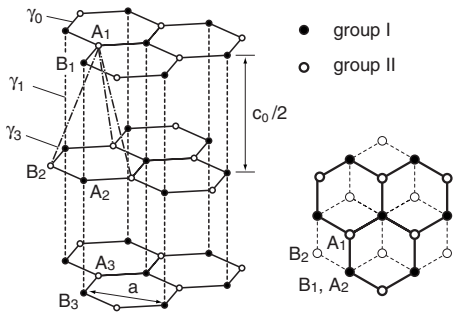

FIG. 1. Atomic structure of multilayer graphene with AB (Bernal) stacking.

model.[25,33–35] The low energy spectrum is given by the states in the vicinity of K and K' points in the Brillouin zone. Let $|A_j\rangle$ and $|B_j\rangle$ be the Bloch functions at the K point, corresponding to the A and B sublattices, respectively, of layer j. For monolayer graphene, the Hamiltonian around K point for the basis $|A_1\rangle$, $|B_1\rangle$ is written as[4,5,13,36,37]

$$H_0 = \begin{pmatrix} 0 & \gamma k_- \\ \gamma k_+ & 0 \end{pmatrix}, \tag{3}$$

where $k_\pm = k_x \pm i k_y$ and

$$\gamma = \frac{\sqrt{3}}{2} a \gamma_0, \tag{4}$$

with γ_0 being the nearest-neighbor coupling in a single layer. We cite the experimental estimation $\gamma_0 \approx 3.16$ eV.[39]

For the interlayer coupling, we include parameters γ_1 and γ_3, following the Hamiltonian previously derived for a bilayer graphene.[16,18] Here, γ_1 represents the coupling between vertically neighboring atoms in group I ($A_{2k} \leftrightarrow B_{2k\pm1}$), and γ_3 between group II atoms on neighboring layers ($B_{2k} \leftrightarrow A_{2k\pm1}$), which are estimated to $\gamma_1 \approx 0.39$ eV (Ref. 40) and $\gamma_3 \approx 0.315$ eV.[41] If we look at the interaction between layers 1 and 2, the matrix element $\langle A_2|\mathcal{H}|B_1\rangle$, corresponding to the vertical bond, becomes γ_1 not accompanying an in-plane Bloch number. The matrix element $\langle B_2|\mathcal{H}|A_1\rangle$ is written as $\gamma' k_+$ with

$$\gamma' = \frac{\sqrt{3}}{2} a \gamma_3, \tag{5}$$

similar to the intralayer term $\langle A_1|\mathcal{H}|B_1\rangle$, as the in-plane vector components from A_1 to B_2 are identical to those from B_1 to A_1.

Accordingly, if the basis is taken as $|A_1\rangle, |B_1\rangle; |A_2\rangle, |B_2\rangle; \ldots; |A_N\rangle, |B_N\rangle$, the Hamiltonian for the multilayer graphene around the K point becomes

$$\mathcal{H} = \begin{pmatrix} H_0 & V & & & \\ V^\dagger & H_0 & V^\dagger & & \\ & V & H_0 & V & \\ & & \ddots & \ddots & \ddots \end{pmatrix}, \tag{6}$$

with

$$V = \begin{pmatrix} 0 & \gamma' k_+ \\ \gamma_1 & 0 \end{pmatrix}. \tag{7}$$

The effective Hamiltonian for K' is obtained by exchanging k_+ and k_- and replacing γ_1 with $-\gamma_1$. The derivation of the effective Hamiltonian based on a tight-binding model is presented in Appendix A.

We show in the following that the Hamiltonian matrix [Eq. (6)] can be block diagonalized into smaller matrices by choosing an appropriate basis independent of $\mathbf{k}$. First, we arrange the basis in the order of group I and then group II, i.e., $|B_1\rangle, |A_2\rangle, |B_3\rangle, \ldots; |A_1\rangle, |B_2\rangle, |A_3\rangle, \ldots$. Then, Eq. (6) becomes

$$\mathcal{H} = \begin{pmatrix} \mathcal{H}_{11} & \mathcal{H}_{12} \\ \mathcal{H}_{12}^\dagger & \mathcal{H}_{22} \end{pmatrix}, \tag{8}$$

with $\mathcal{H}_{ij}$ being $N \times N$ matrices defined as

$$\mathcal{H}_{11} = \gamma_1 \begin{pmatrix} 0 & 1 & & & & \\ 1 & 0 & 1 & & & \\ & \ddots & \ddots & \ddots & & \\ & & & 1 & 0 & 1 \\ & & & & 1 & 0 \end{pmatrix}, \tag{9}$$

$$\mathcal{H}_{12} = \gamma \begin{pmatrix} k_+ & & & & \\ & k_- & & & \\ & & k_+ & & \\ & & & \ddots & \\ & & & & k_\pm \end{pmatrix}, \tag{10}$$

$$\mathcal{H}_{22} = \gamma' \begin{pmatrix} 0 & k_+ & & & & \\ k_- & 0 & k_- & & & \\ & k_+ & 0 & k_+ & & \\ & & \ddots & \ddots & \ddots & \\ & & & k_\mp & 0 & k_\mp \\ & & & & k_\pm & 0 \end{pmatrix}, \tag{11}$$

where the upper and lower signs correspond to odd and even N, respectively.

If we set $\mathbf{k}=0$ (the K point), $\mathcal{H}_{12}$ and $\mathcal{H}_{22}$ vanish. Remaining $\mathcal{H}_{11}$ is equivalent to the Hamiltonian of a one-dimensional tight-binding chain with the nearest-neighbor coupling γ_1, giving a set of eigenenergies

$$\varepsilon_m = \gamma_1 \lambda_{N,m},$$

$$\lambda_{N,m} = 2 \sin \frac{m\pi}{2(N+1)}, \tag{12}$$

with

$$m = -(N-1), -(N-3), \ldots, N-1. \tag{13}$$

Here, m is an odd integer when the layer number N is even, while m is even when N is odd, and therefore $m=0$ is allowed only for odd N.

The corresponding wave function is explicitly written as

$$\psi_m(j) = \sqrt{\frac{2}{N+1}} \sin\left[\frac{(-m+N+1)\pi}{2(N+1)} j\right], \tag{14}$$

where $\psi_m(j)$ represents the amplitudes at $|B_1\rangle, |A_2\rangle, |B_3\rangle, \ldots$ and satisfies

$$\sum_j \psi_m(j)\psi_{m'}(j) = \delta_{mm'}. \tag{15}$$

We have a relation between the wave functions ψ_m and ψ_{-m} as

$$\psi_{-m}(j) = \psi_m(j)(-1)^{j+1}. \tag{16}$$

Now, we construct the basis by assigning $\psi_m(j)$ to the atoms of groups I and II as

$$|\phi_m^{(\mathrm{I})}\rangle = \psi_m(1)|B_1\rangle + \psi_m(2)|A_2\rangle + \psi_m(3)|B_3\rangle + \cdots,$$

$$|\phi_m^{(\mathrm{II})}\rangle = \psi_m(1)|A_1\rangle + \psi_m(2)|B_2\rangle + \psi_m(3)|A_3\rangle + \cdots \quad (17)$$

and attempt to rewrite the Hamiltonian [Eq. (6)]. The matrix elements within group I come from $\mathcal{H}_{11}$ and become diagonal as is obvious from the definition,

$$\langle\phi_{m'}^{(\mathrm{I})}|\mathcal{H}|\phi_m^{(\mathrm{I})}\rangle = \delta_{m,m'}\gamma_1\lambda_{N,m}. \quad (18)$$

Off-diagonal elements between $|\phi_m^{(\mathrm{I})}\rangle$ and $|\phi_{m'}^{(\mathrm{II})}\rangle$ are written from $\mathcal{H}_{12}$ as

$$\langle\phi_{m'}^{(\mathrm{II})}|\mathcal{H}|\phi_m^{(\mathrm{I})}\rangle = \gamma k_x \sum_{j=1}^{N} \psi_{m'}^*(j)\psi_m(j) + i\gamma k_y \sum_{j=1}^{N} \psi_{m'}^*(j)\psi_m(j) \times(-1)^j = \gamma(k_x\delta_{m,m'} - ik_y\delta_{m,-m'}). \quad (19)$$

In the second equality, we used relation (16) and orthogonality (15). Lastly, the matrix elements within group II are obtained from $\mathcal{H}_{22}$ as

$$\begin{aligned}\langle\phi_{m'}^{(\mathrm{II})}|\mathcal{H}|\phi_m^{(\mathrm{II})}\rangle &= \gamma' k_x \sum_{j=1}^{N-1} [\psi_{m'}^*(j+1)\psi_m(j) + \psi_{m'}^*(j)\psi_m(j+1)] \\ &+ \gamma' i k_y \sum_{j=1}^{N-1} (-1)^j [\psi_{m'}^*(j+1)\psi_m(j) \\ &- \psi_{m'}^*(j)\psi_m(j+1)] \\ &= \gamma'\lambda_{N,m}(k_x\delta_{m,m'} + ik_y\delta_{m,-m'}). \end{aligned} \quad (20)$$

The Hamiltonian is thus closed in the subspace $\{|\phi_m^{(\mathrm{I})}\rangle, |\phi_{-m}^{(\mathrm{I})}\rangle, |\phi_m^{(\mathrm{II})}\rangle, |\phi_{-m}^{(\mathrm{II})}\rangle\}$ for each $|m|$. Particularly, $m=0$ is special in that the subspace is spanned with only two bases $\{|\phi_0^{(\mathrm{II})}\rangle, |\phi_0^{(\mathrm{I})}\rangle\}$, while this is absent in even-layer graphenes. The submatrix is written as

$$\mathcal{H}_{m=0} = \begin{pmatrix} 0 & \gamma k_- \\ \gamma k_+ & 0 \end{pmatrix}, \quad (21)$$

which is independent of γ_1 and γ_3 and equivalent to the Hamiltonian of the monolayer graphene.

For $m \neq 0$, we rearrange the basis as

$$\{(|\phi_m^{(\mathrm{II})}\rangle + |\phi_{-m}^{(\mathrm{II})}\rangle)/\sqrt{2}, (|\phi_m^{(\mathrm{I})}\rangle + |\phi_{-m}^{(\mathrm{I})}\rangle)/\sqrt{2}, (|\phi_m^{(\mathrm{I})}\rangle - |\phi_{-m}^{(\mathrm{I})}\rangle)/\sqrt{2}, (|\phi_m^{(\mathrm{II})}\rangle - |\phi_{-m}^{(\mathrm{II})}\rangle)/\sqrt{2}\}, \quad (22)$$

where we take $m>0$ without loss of generality. We then obtain

$$\mathcal{H}_m = \begin{pmatrix} 0 & \gamma k_- & 0 & \lambda\gamma' k_+ \\ \gamma k_+ & 0 & \lambda\gamma_1 & 0 \\ 0 & \lambda\gamma_1 & 0 & \gamma k_- \\ \lambda\gamma' k_- & 0 & \gamma k_+ & 0 \end{pmatrix}, \quad (23)$$

with $\lambda=\lambda_{N,m}$. This is equivalent to the Hamiltonian of a bilayer graphene except that γ_1 and $\gamma'(\propto\gamma_3)$ are multiplied by λ.

Thus, the Hamiltonian of odd-layered graphene is composed of one monolayer-type and $(N-1)/2$ bilayer-type subbands, while that of even-layered graphene is composed of $N/2$ bilayers but no monolayer. The similar idea was previously proposed for trilayer graphene without γ_3, where it was shown that the energy spectrum becomes a superposition of that for a monolayer and for a bilayer.[21] Here, we have extended this argument to decomposition of the Hamiltonian matrix and to systems with arbitrary number of layers including the trigonal warping. We also note that **k** independence of the basis becomes important in the following sections, since this enables us to write the magnetization as a sum over contributions from sub-Hamiltonians, which are independently calculated.

Many other parameters were introduced for the description of the band structure of bulk graphite.[25,26,35,38] The parameter γ_4 couples group I and II atoms sitting on the neighboring layers, such as $A_j \leftrightarrow A_{j+1}$ or $B_j \leftrightarrow B_{j+1}$. This parameter does not change the qualitative feature of the low-energy spectrum and therefore is not important.[25] Parameters γ_2 and γ_5 represent vertical hoppings between the second-nearest neighboring layers for group II and I atoms, respectively. Further, γ_6 is an energy difference between the group I and II atoms due to difference in the chemical environment. Inclusion of these parameters γ_2, γ_5, and γ_6 causes opening up of small energy gaps between the conduction and the valence bands. However, these gaps do not play important roles in the magnetization, as will be discussed in the following.

In 3D limit, $N\to\infty$, the eigenstate becomes a superposition of opposite traveling waves with $\pm k_z$ along the stacking direction. The relation between the index m and $|k_z|$ is obtained by comparing the eigenenergy of $\mathcal{H}_{11}$, Eq. (12), to that of the 3D limit, $2\gamma_1\cos(k_z c_0/2)$, as

$$\frac{|k_z|c_0}{2} = \frac{(-m+N+1)\pi}{2(N+1)}. \quad (24)$$

The band structure of the Hamiltonian [Eq. (23)] can be obtained by replacing γ_1 by $\lambda\gamma_1$ and γ_3 by $\lambda\gamma_3$ in that of the bilayer.[16] We plot in Fig. 2 the dispersion for $\lambda=2$, which has the maximum trigonal warping. The middle two subbands stick together at $\varepsilon=0$, while the remaining two bands appear only in the energy range $|\varepsilon|>\lambda\gamma_1$. If we neglect γ_3, the effective Hamiltonian for $|\varepsilon|\ll\lambda\gamma_1$ becomes

$$\mathcal{H} = \frac{\hbar^2}{2m^*}\begin{pmatrix} 0 & k_-^2 \\ k_+^2 & 0 \end{pmatrix}, \quad (25)$$

which works for the reduced basis

$$\{(|\phi_m^{(\mathrm{II})}\rangle + |\phi_{-m}^{(\mathrm{II})}\rangle)/\sqrt{2}, (|\phi_m^{(\mathrm{II})}\rangle - |\phi_{-m}^{(\mathrm{II})}\rangle)/\sqrt{2}\}, \quad (26)$$

giving a rotationally symmetric dispersion with the effective mass,

$$m^* = \frac{\hbar^2(\lambda\gamma_1)}{2\gamma^2}. \quad (27)$$

The term proportional to γ_3 is responsible for the trigonal warping effect, which is most remarkable around the band sticking point $\varepsilon=0$. Let us define

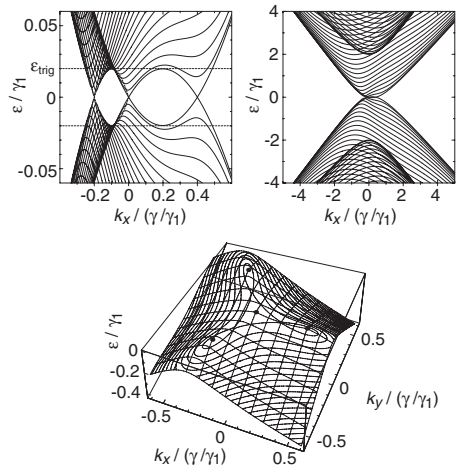

FIG. 2. (Top) Projected band structure of the sub-Hamiltonian [Eq. (23)] with $\lambda=2$ and $\gamma_3/\gamma_0=0.1$. $|\varepsilon|=\varepsilon_{trig}=0.02\gamma_1$ is shown as horizontal dotted lines. Right panel shows zoom out of the left. (Bottom) 3D plot of the lower second band around the band touching point. Four Fermi points at $\varepsilon=0$ indicated by dots.

$$\varepsilon_{trig} = \frac{1}{4}\left(\frac{\lambda\gamma_3}{\gamma_0}\right)^2(\lambda\gamma_1). \tag{28}$$

In the energy range $|\varepsilon| \lesssim \varepsilon_{trig}$, the Fermi line splits into four separated pockets, one center part and three leg parts located trigonally, which shrink into four Fermi points linearly with $\varepsilon \to 0$. We note that ε_{trig} is proportional to λ^3 and thus very sensitive to λ, while the energy of the higher-band bottom, $\lambda\gamma_1$, behaves linear to λ. The maximum of λ approaches 2 as the layer number increases, so that ε_{trig} becomes as large as $2(\gamma_3/\gamma_0)^2\gamma_1 \approx 8$ meV.

Figure 3 shows the band structures around the K point along the k_x axis in the multilayer graphenes with $N=2$, 3, 4, and 5 and $\gamma_3/\gamma_0=0.1$. The lists of $\lambda_{N,m}$ are given as

$$N=1:\ \{\lambda_{1,0}\}=\{0\},$$

$$N=2:\ \{\lambda_{2,1}\}=\{1\},$$

$$N=3:\ \{\lambda_{3,0},\lambda_{3,2}\}=\{0,\sqrt{2}\},$$

$$N=4:\ \{\lambda_{4,1},\lambda_{4,3}\}=\{(\sqrt{5}-1)/2,(\sqrt{5}+1)/2\},$$

$$N=5:\ \{\lambda_{5,0},\lambda_{5,2},\lambda_{5,4}\}=\{0,1,\sqrt{3}\}. \tag{29}$$

While we have included γ_0, γ_1, and γ_3 in our graphene model, the extra parameter neglected here may make some changes in the electronic structure. The energy band of a few-layered graphene has been calculated in the density functional calculation[22] and the tight-binding model.[23,24] Those results differ from ours, mainly in that the band centers relatively shift depending on m and that a narrow gap opens, where the conduction and valence bands (within a single m) touch and where different bands (with different m's) cross. Gaps are attributed to effects of couplings such as γ_2, γ_5, and γ_6, which are mentioned above. In terms of the effective mass Hamiltonian [Eq. (6)], those parameters appear as matrix elements without being multiplied by the wave number k_x and k_y, since they are associated with a hopping along the z axis or a diagonal element. Thus, they do not vanish at $k=0$ (K or K') and lift the degeneracy to open a gap. Apart from the gap opening, the main feature of the trigonal warping is well described in the present model. It should also be mentioned that an energy gap is induced by an electric field perpendicular to the layer stacking direction,[15,17,21,42] where the electrostatic potential appears as matrix elements independent of k_x and k_y as well.

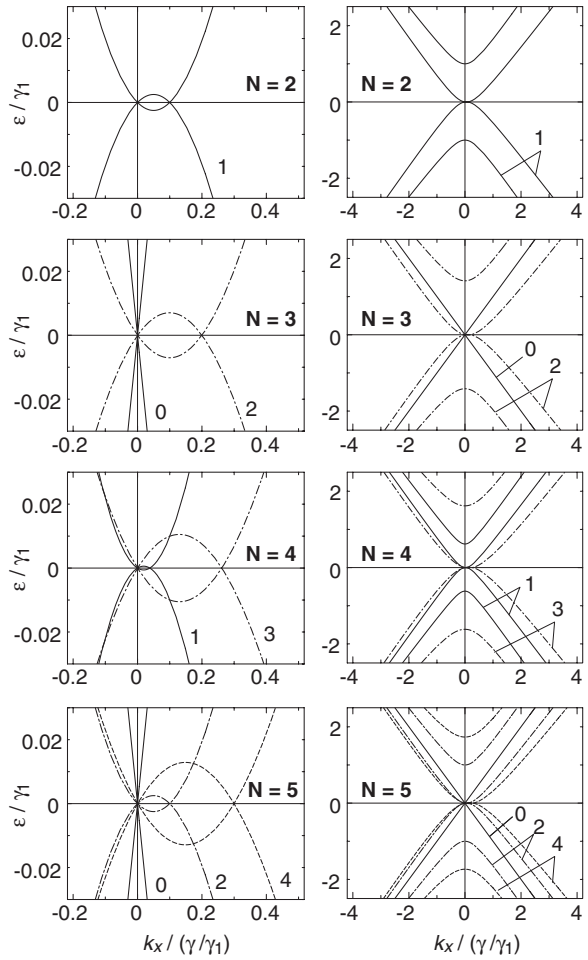

FIG. 3. Band structures of multilayer graphenes, $N=2,3,4,5$ with $\gamma_3/\gamma_0=0.1$, around the K point (taken as origin) along the k_x axis. Right panel shows a zoom out of the left. Numbers assigned to curves indicate m.

III. MAGNETISM OF MULTILAYER GRAPHENES

For the magnetic susceptibility, we use the general expression based on the linear response theory,[44]

$$\chi = \mathrm{Im}\int_{-\infty}^{\infty} d\varepsilon f(\varepsilon)F(\varepsilon+i0), \tag{30}$$

with

$$F(z) = -\frac{g_v g_s}{2\pi L^2}\frac{e^2}{\hbar^2}\sum_{\mathbf{k}} \mathrm{tr}(G\mathcal{H}_x G\mathcal{H}_y G\mathcal{H}_x G\mathcal{H}_y), \qquad (31)$$

where $g_v=2$ is the valley degeneracy, $g_s=2$ is the spin degeneracy, and L is the system size. We defined here $\mathcal{H}_x = \partial\mathcal{H}/\partial k_x$, $\mathcal{H}_y = \partial\mathcal{H}/\partial k_y$, $G(z)=(z-\mathcal{H})^{-1}$, and $f(\varepsilon)=[1+e^{(\varepsilon-\mu)/k_BT}]^{-1}$, with the chemical potential μ and the temperature T. The formula valid also for the Hamiltonian [Eq. (25)] is discussed in Appendix B. By integration by parts in Eq. (30), we have

$$\chi(T,\mu) = \int_{-\infty}^{\infty} d\varepsilon \left(-\frac{\partial f}{\partial \varepsilon}\right)\chi(0,\varepsilon), \qquad (32)$$

showing that the susceptibility at nonzero temperature is written in terms of that at zero temperature. The integration of χ over μ is independent of T.

We include the impurity scattering effects by introducing a self-energy $-i\Gamma$ in the Green's function, i.e., $i0$ in Eq. (30) is replaced by $i\Gamma$. Here, we simply assume the scattering rate $\Gamma=\hbar/2\tau$ to be independent of energy.

Using the decomposition of the Hamiltonian, the magnetization of the N-layered graphene can be written as a summation over each sub-Hamiltonian. The contribution from $m=0$ is exactly equivalent to the susceptibility of a monolayer graphene,[4,26] which becomes at zero temperature and in the clean limit,

$$\chi_{\mathrm{mono}} = -\frac{g_v g_s}{6\pi}\frac{e^2\gamma^2}{\hbar^2}\delta(\varepsilon_F). \qquad (33)$$

Thus, the odd-layer graphene always has a large diamagnetic peak at zero energy. The delta-function dependence of χ_{mono} agrees with the general property of the susceptibility in systems described by the k-linear Hamiltonian, as discussed in Sec. IV.

In the presence of disorder, the delta function is broadened into a Lorentzian with width Γ and the same area,[31] i.e.,

$$\chi_{\mathrm{mono}} = -\frac{g_v g_s}{6\pi}\frac{e^2\gamma^2}{\hbar^2}\frac{\Gamma}{\pi(\varepsilon_F^2+\Gamma^2)}, \qquad (34)$$

within the present model assuming a constant Γ. The shape of the peak itself depends on the model disorder and we may have some different manner of broadening in a more realistic treatment. In fact, in the monolayer graphene, it was shown in a self-consistent Born approximation[8] that χ has a much sharper peak at $\varepsilon=0$ than the Lorentzian and also a large tail proportional to $|\varepsilon|^{-1}$ for $\varepsilon\neq 0$.[32] In multilayer cases, effects of disorder are more complicated because of the presence of other bands. This problem is out of the scope of this work.

The susceptibility of a bilayer graphene described by the Hamiltonian [Eq. (23)] was analytically calculated for the case of $\gamma_3=0$.[28] The expression for $T=0$ and $\Gamma=0$ is given by

$$\chi = -\frac{g_v g_s}{4\pi}\frac{e^2\gamma^2}{\hbar^2}\frac{\theta(\lambda\gamma_1-|\varepsilon_F|)}{\lambda\gamma_1}\left(-\ln\frac{|\varepsilon_F|}{\lambda\gamma_1}-\frac{1}{3}\right), \qquad (35)$$

with $\lambda=\lambda_{N,m}$, where $\theta(t)$ is a step function defined by

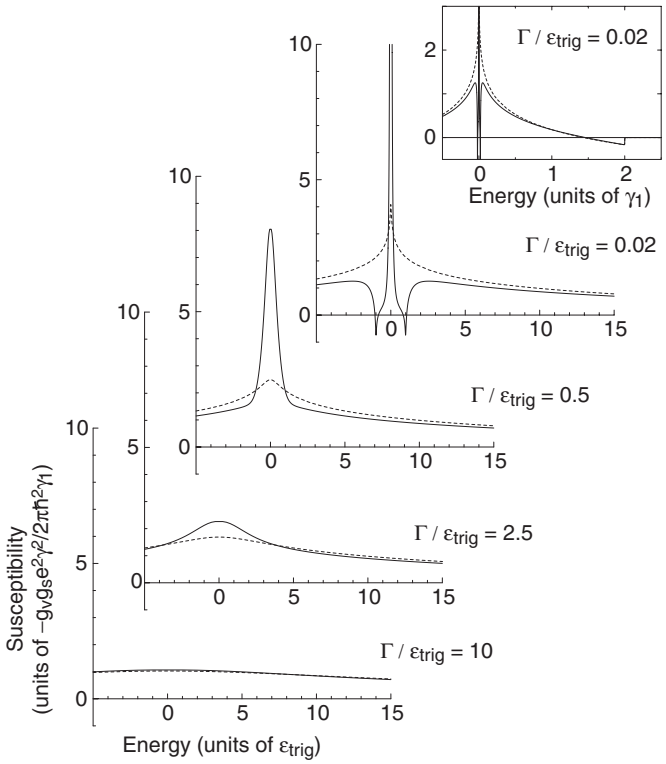

FIG. 4. Susceptibility of the sub-Hamiltonian [Eq. (23)] in the multilayer graphene with $\lambda_{N,m}=2$, $\gamma_3/\gamma_0=0.1$, and several disorder strengths Γ. Energy is scaled in units of $\varepsilon_{\mathrm{trig}}=0.02\gamma_1$. Dashed curves show plots for $\gamma_3=0$. Inset at the top is a zoom out of the top panel ($\Gamma=0.02\varepsilon_{\mathrm{trig}}$) with units of energy γ_1.

$$\theta(t) = \begin{cases} 1 & (t>0) \\ 0 & (t<0). \end{cases} \qquad (36)$$

The susceptibility diverges logarithmically toward $\varepsilon_F=0$, becomes slightly positive for $|\varepsilon_F|<\sim\lambda\gamma_1$, and vanishes for $|\varepsilon_F|>\lambda\gamma_1$, where the higher subband enters. In the presence of disorder, the logarithmic peak is broadened approximately as $\propto\ln\sqrt{\varepsilon_F^2+\Gamma^2}$.

The integration of χ in Eq. (35) over the Fermi energy becomes $-(g_v g_s/3\pi)(e^2\gamma^2/\hbar^2)$ independent of γ_1, which is exactly twice as large as that of the monolayer graphene [Eq. (33)]. This arises due to the fact that the integral of χ over the Fermi energy is determined only by terms of the Hamiltonian matrix, proportional to k_x or k_y, and is independent of terms independent of k_x and k_y. A proof of this important property is presented in Sec. IV.

If we include the extra band parameter γ_3, the low-energy structure of the susceptibility [Eq. (35)] drastically changes due to the fine structure around the band touching point. To demonstrate this, we numerically calculate χ for the Hamiltonian [Eq. (23)] in the case of the maximum trigonal warping, $\lambda_{N,m}=2$. Figure 4 shows the susceptibility as a function of ε_F with several values of Γ. We take $\gamma_3/\gamma_1=0.1$, where the Fermi line splitting occurs in lower than $\varepsilon_{\mathrm{trig}}=0.02\gamma_1$. For reference, we also plot the result without the trigonal warping, $\gamma_3=0$, as a dashed curve.

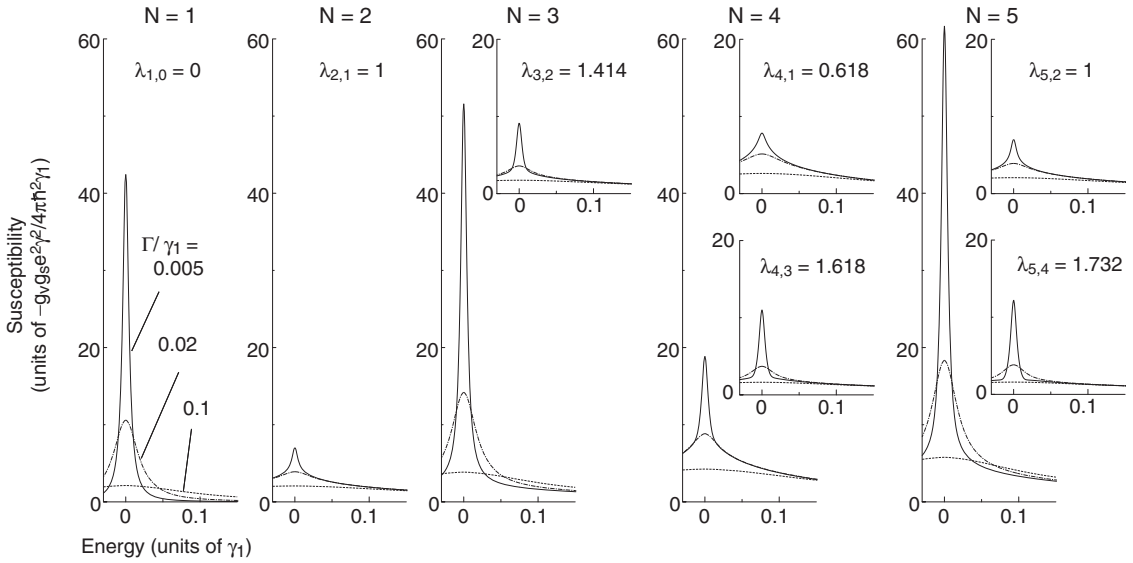

FIG. 5. Susceptibility of multilayer graphenes with layer numbers $N=1-5$ plotted against the Fermi energy. Results shown for several disorder strengths specified by constant scattering rate Γ.

When we go down from high energy in the top panel (the smallest Γ), the susceptibility gradually deviates downward from the logarithmic dependence of $\gamma_3=0$ and takes a sharp dip at $\varepsilon=\varepsilon_{\rm trig}$. Remarkably, we have a strong peak centered on $\varepsilon=0$, which is regarded as the effect of the linear dispersions around zero energy. The integral of χ over the Fermi energy is almost constant $-(g_v g_s/3\pi)(e^2\gamma^2/\hbar^2)$, as discussed in Sec. IV, showing that the reduction in higher energies compensates the zero-energy peak. As Γ becomes larger, the peak begins to cancel with the reduction in high energy and the effect of γ_3 eventually disappears when $\Gamma \gg \varepsilon_{\rm trig}$. In contrast, the peak associated with the monolayer band $m=0$ becomes broad in Γ but never vanishes, as shown in Eq. (34).

Figure 5 shows $\chi(\varepsilon_F)$ of graphenes with layer number from $N=1$ to 5 with several disorder strengths Γ. For $N \geqslant 3$, insets show the contributions from each of bilayer-type bands. The result of odd N always contains a monolayerlike component, which is exactly the same as $N=1$ and thus omitted in the inset. We can see that odd-layered graphenes exhibit a particularly large peak, which mainly comes from the monolayertype band. A bilayerlike component contains a central peak due to the trigonal warping and a logarithmic tail in high energies, in accordance with Fig. 4.

The layer-number dependence of the susceptibility in multilayer graphene has been studied for the graphite intercalation compounds.[29] This system can be viewed as independent multilayer graphenes bound by the intercalant layers, but the intercalants give a strong electrostatic potential along the stacking direction, leading to the charge redistribution among different layers.[43] As a result, the band structure and the magnetization are considerably different from our system with a uniform electrostatic potential in the vertical direction.

In isolated multilayer graphenes realized in recent experiments, we may have some potential difference among layers depending on the experimental environment, and this can also be tuned by the external electric field as mentioned. In Sec. IV, we will show that, as long as the potential is not too strong to alter the entire band structure, this does not change the qualitative feature of the magnetization.

IV. DISCUSSION

The zero-energy peak in the bilayer-type subband originates in Dirac-like dispersions appearing around four Fermi points. Using the known results in a bilayer,[16] we can show that the sequence of the Landau levels in the center pocket approximately becomes $\varepsilon=\mathrm{sgn}(n)(\sqrt{2}\lambda_{N,m}\gamma'/l)\sqrt{|n|}$ with $N=0,1,2,\ldots$, and those in the three leg parts $\varepsilon=\mathrm{sgn}(n)\times(\sqrt{6}\lambda_{N,m}\gamma'/l)\sqrt{|n|}$, where $l=\sqrt{\hbar/(eB)}$ is the magnetic length. Since the susceptibility is determined solely by Landau-level energies, we compare this to the monolayer's sequence $\varepsilon=\mathrm{sgn}(n)(\sqrt{2}\gamma/l)\sqrt{|n|}$ and obtain χ from each pocket by substituting γ in Eq. (33). We end up with

$$\chi = 10\left(\frac{\lambda_{N,m}\gamma_3}{\gamma_0}\right)^2 \chi_{\rm mono}, \tag{37}$$

except for a constant coming from the integral over the lower energy states. The zero-energy peak in Fig. 4 fits well to the Lorentzian with width Γ and the area of the delta function [Eq. (37)], as long as $\Gamma < \sim \varepsilon_{\rm trig}$.

The factor attached to $\chi_{\rm mono}$ becomes as large as 0.4 when $\lambda_{N,m}=2$ and $\gamma_3/\gamma_0=0.1$, and therefore the singularity is not too small compared with that of the monolayer. For N-layered graphene, a simple relation,

$$\sum_{\lambda_{N,m}>0} (\lambda_{N,m})^2 = N-1, \tag{38}$$

leads to the summation of Eq. (37) over all the bilayer-type subbands,

$$\chi = 10(N-1)\left(\frac{\gamma_3}{\gamma_0}\right)^2 \chi_{\text{mono}} \approx 0.1(N-1)\chi_{\text{mono}}. \quad (39)$$

In Fig. 5, the peak height becomes a little larger than this estimation due to mixing with the logarithmic tail.

The delta-function dependence of χ in monolayer graphene is a characteristic property common to general k-linear Hamiltonian. This can be shown using the scaling argument. We consider a Hamiltonian $\mathcal{H}$ which contains only terms linear in k_x and k_y. We change the energy and wave number scales by an arbitrary factor α as

$$\varepsilon = \alpha\tilde{\varepsilon}, \quad k_i = \alpha\tilde{k}_i, \quad (40)$$

then the Hamiltonian becomes formally identical under this transformation, since the coefficients of k-linear terms in the Hamiltonian remain unchanged.

Going back to the definition of χ in Eqs. (30) and (31), $F(z)$ is scaled as

$$F(z) = \frac{1}{\alpha^2}\tilde{F}(\tilde{z}). \quad (41)$$

The function F should depend only on the coefficients of k-linear terms and natural constants and thus is invariant under the scale transformation, namely, we have $F=\tilde{F}$. With Eq. (41), we come up with an equation,

$$F(z) = \frac{1}{\alpha^2}F\left(\frac{z}{\alpha}\right), \quad (42)$$

which is satisfied solely by

$$F(z) = \frac{A}{z^2}. \quad (43)$$

A constant A is related to the integral of the susceptibility $\chi(\varepsilon_F)$ over the Fermi energy ε_F. From Eq. (30), we generally have

$$\int_{-\infty}^{\infty}\chi(\varepsilon)d\varepsilon = -\,\text{Im}\int_{-\infty}^{\infty}d\varepsilon\varepsilon F(\varepsilon+i0) = \frac{1}{2i}\oint_C dzzF(z), \quad (44)$$

where the integral path C is a circle with an infinite radius with counterclockwise direction. In the present system, Eq. (43) immediately gives the integral as πA. This is an integral of the real function $\chi(\varepsilon)$ and thus is real. Substituting Eq. (43) with real A in Eq. (30), we finally obtain the explicit form of the zero-temperature susceptibility as

$$\chi(\varepsilon_F) = -\,\text{Im}\frac{A}{\varepsilon_F+i0} = \pi A\,\delta(\varepsilon_F). \quad (45)$$

As discussed in Sec. II, the band structure in more realistic models has an energy gap around zero energy due to extra band parameters neglected in the present model. It was also mentioned that the external electric field along the stacking direction opens an energy gap. One might think that the gap would strongly reduce the large diamagnetism at the band touching point. However, we can show within the effective mass approximation that the integral of susceptibility over ε_F is independent of any kind of matrix elements without k_x and k_y, which are responsible for gap opening. This is obvious from the general expression [Eq. (44)]; even if the Hamiltonian contains k-independent terms in addition to k-linear terms, they can be safely neglected in the integral as they are infinitesimal compared to $|z|$ on the path C. In the effective mass model of the multilayer graphene, we immediately conclude that the integral is independent of γ_1, γ_2, γ_5, γ_6, and any other parameters independent of the wave vector. Thus, we expect that the large diamagnetic peak is still visible even when a gap opens, while it may get broadened in energy by the gap width. The diamagnetism in narrow gap systems is known in bismuth[45] and recently studied for the gapped Dirac fermion.[46] Any further discussion requires a direct computation of the magnetization including extra parameters, but we leave this for the future study.

The integral of the susceptibility can be calculated by the Hamiltonian with the k-independent terms dropped and thus depends only on the band parameters associated with k-linear terms. In our model [Eq. (6)], the value is mainly determined by the dominant parameter γ_0, while γ_3 gives a correction at most of the order of $(\gamma_3/\gamma_0)^2 \sim 0.01$. The correction must be the second order in γ_3 because we can change γ_3 to $-\gamma_3$ in the Hamiltonian with a unitary transformation multiplying the base on layer j by $(-1)^j$. As a result, the integral of $\chi(\varepsilon_F)$ for the bilayer-type Hamiltonian becomes almost twice as large as the monolayer's, and the summation over all the subsystems in N-layered graphene becomes approximately N times as large as the monolayer's.

It is instructive to derive the susceptibility starting from the Landau-level energies. In the monolayer graphene, the thermodynamic function Ω is given by

$$\Omega = -k_B T g_v g_s \frac{1}{2\pi l^2}\sum_n g(\varepsilon_n)\varphi(\varepsilon_n), \quad (46)$$

$$\varphi(\varepsilon) = \ln\{1+\exp[\beta(\mu-\varepsilon)]\}, \quad (47)$$

where $\beta = 1/k_B T$, $\varepsilon_n = \text{sgn}(n)\hbar\omega_B\sqrt{|n|}$ with $\hbar\omega_B = \sqrt{2}\gamma/l$, and $g(\varepsilon)$ a cutoff function which gradually decays to zero for $|\varepsilon| \gtrsim \varepsilon_c$ with cutoff energy ε_c. We can rewrite this as

$$\Omega = -k_B T g_v g_s \frac{1}{2\pi l^2}\sum_{n=0}^{\infty}\left(1-\frac{1}{2}\delta_{n0}\right)H(nh), \quad (48)$$

where

$$H(x) = g(\sqrt{x})\ln[1+2\exp(\beta\mu)\cosh(\beta\sqrt{x})+\exp(2\beta\mu)], \quad (49)$$

with $h=(\hbar\omega_B)^2$.

Expanding the integral

$$\int_0^{\infty}H(x)dx = \int_0^{h/2}H(x)dx + \sum_{j=1}^{\infty}\int_{-h/2}^{h/2}H(x+hj)dx, \quad (50)$$

with respect to h, we immediately have

$$h\left[\frac{1}{2}H(0)+\sum_{j=1}^{\infty}H(x+hj)\right]=\int_0^{\infty}H(x)dx-\frac{1}{12}h^2\left[H'(0)+\frac{1}{2}H'(\infty)\right], \quad (51)$$

up to the second order in h or in B. Then, we have

$$\Omega=\Omega_0+\Delta\Omega, \quad (52)$$

where Ω_0 is the thermodynamic function in the absence of a magnetic field and

$$\Delta\Omega=\frac{1}{12}\frac{g_v g_s(\hbar\omega_B)^2}{2\pi l^2}\frac{\beta\exp(\beta\zeta)}{[1+\exp(\beta\zeta)]^2}=\frac{g_v g_s\gamma^2}{12\pi l^4}\int_{-\infty}^{\infty}\left[-\frac{\partial f(\varepsilon)}{\partial\varepsilon}\right]\delta(\varepsilon)d\varepsilon. \quad (53)$$

Applying the relation $\Delta\Omega=\chi B^2/2$, we obtain χ_{mono} given by Eq. (33) at zero temperature.

We should note that the thermodynamic function in the absence of a magnetic field is given by

$$\Omega_0=-k_BTg_v g_s\frac{1}{2\pi l^2}\sum_n\int_{-1/2}^{1/2}g(\varepsilon_{n+t})\varphi(\varepsilon_{n+t})dt. \quad (54)$$

For contributions of states with $|n|\gg 1$, we can expand the above with respect to t and have to the lowest order in the field strength B,

$$\begin{aligned}\Delta\Omega&=\frac{g_v g_s}{2\pi l^2}\frac{1}{96}(\hbar\omega_B)^4\sum_{|n|\gg 0}[\varepsilon_n^{-3}f(\varepsilon_n)-\varepsilon_n^{-2}f'(\varepsilon_n)]\\&\approx\frac{g_v g_s}{2\pi l^2}\frac{(\hbar\omega_B)^2}{48}\lim_{\delta\to+0}\left\{\int_{\delta}^{\infty}[\varepsilon^{-2}f(\varepsilon)-\varepsilon^{-1}f'(\varepsilon)]d\varepsilon-\int_{-\infty}^{-\delta}[\varepsilon^{-2}f(\varepsilon)-\varepsilon^{-1}f'(\varepsilon))d\varepsilon\right\}\\&=-\frac{g_v g_s}{2\pi l^2}\frac{1}{24}(\hbar\omega_B)^2\int_{-\infty}^{\infty}\left[-\frac{\partial f(\varepsilon)}{\partial\varepsilon}\right]\delta(\varepsilon)d\varepsilon. \quad (55)\end{aligned}$$

This gives a "paramagnetic" susceptibility. For $n=0$, on the other hand, the change in the thermodynamic potential is calculated as

$$\Delta\Omega=\frac{g_v g_s}{2\pi l^2}\frac{1}{8}(\hbar\omega_B)^2\int_{-\infty}^{\infty}\left[-\frac{\partial f(\varepsilon)}{\partial\varepsilon}\right]\delta(\varepsilon)d\varepsilon. \quad (56)$$

The sum of these two contribution is the same as Eq. (53), as is expected.

In the bilayer graphene, the Landau level with $\gamma_3=0$ in the region $|\varepsilon|\ll\gamma_1$ can be calculated from the Hamiltonian [Eq. (25)] as[16]

$$\varepsilon_{sn}=s\hbar\omega_c\sqrt{n(n+1)}, \quad (57)$$

where $\omega_c=eB/m^*$ with m^* defined in Eq. (27), $s=\pm 1$, and $n=0,1,2,\ldots$. We have doubly degenerate levels at zero energy ($n=0$, $s=\pm 1$), while the spacing gradually becomes constant as n goes higher. In a similar but more complicated manner, the susceptibility is calculated as

$$\chi=-\left(\frac{e\hbar}{2m^*}\right)^2\frac{g_v g_s m^*}{2\pi\hbar^2}\int_{-\infty}^{\infty}g(\varepsilon)\ln\frac{\varepsilon_c}{e|\varepsilon|}\left(-\frac{\partial f}{\partial\varepsilon}\right)d\varepsilon, \quad (58)$$

which correctly describes the logarithmic divergence around zero energy in the rigorous expression [Eq. (35)], as expected. A constant term independent of energy is missing in Eq. (58) since this depends on all the low-energy bands which are neglected in this calculation.

We can understand the logarithmic dependence intuitively by looking into the Landau level sequence. The Landau-level energy can be expanded for large n as

$$\varepsilon_{sn}=s\hbar\omega_c\left[\left(n+\frac{1}{2}\right)-\frac{1}{8}\left(n+\frac{1}{2}\right)^{-1}+\cdots\right], \quad (59)$$

where the first term gives the constant interval, and the second gives a shift toward zero energy, which is rewritten as $-(\hbar\omega_c)^2/(8\varepsilon_{sn})$. For $\varepsilon_F<0$, for example, the change in the total energy due to the energy shift is calculated as

$$\Delta E=-\frac{g_v g_s m^*}{2\pi\hbar^2}\int_{-\varepsilon_c}^{\varepsilon_F}\frac{(\hbar\omega_c)^2}{8\varepsilon}d\varepsilon=\frac{B^2}{2}\frac{g_v g_s}{4\pi}\frac{e^2\gamma^2}{\hbar^2\lambda\gamma_1}\ln\frac{\varepsilon_c}{|\varepsilon_F|}, \quad (60)$$

giving the $\ln|\varepsilon_F|$ dependence of the susceptibility.

For the Hamiltonian [Eq. (25)] containing terms proportional to $k_{\pm}^2$, the susceptibility formula [Eq. (30)] with Eq. (31) is no longer valid, since this was originally derived for systems in which x commutes with $\mathcal{H}_y$ and $\mathcal{H}_{yy}=\partial^2\mathcal{H}/\partial k_y^2$. The modified formula should be

$$F(z)=-\frac{g_v g_s}{4\pi L^2}\frac{e^2}{\hbar^2}\sum_{\mathbf{k}}\mathrm{tr}\left(G\mathcal{H}_xG\mathcal{H}_yG\mathcal{H}_xG\mathcal{H}_y-2G\mathcal{H}_xG\mathcal{H}_xG\mathcal{H}_yG\mathcal{H}_y-\frac{1}{2}G\mathcal{H}_yG\mathcal{H}_{xx}G\mathcal{H}_y-\frac{1}{2}G\mathcal{H}_xG\mathcal{H}_{yy}G\mathcal{H}_x\right). \quad (61)$$

This is derived in Appendix B. A scaling argument similar to the case of the monolayer graphene then gives $F(z)\propto 1/z$. This again leads to the logarithmic dependence of χ on the Fermi energy, which coincides with Eq. (58) apart from a constant.

The experimental measurements of the magnetization of two-dimensional electron systems were performed on the semiconductor heterostructures by using the superconducting quantum interference device[47,48] or using the torque magnetometer.[49–51] We expect that the detection of the graphene magnetism is also feasible with those techniques.

We have studied the orbital magnetism of multilayer graphene with the Bernal stacking in the effective mass approximation. We have demonstrated that the Hamiltonian and thus the susceptibility can be decomposed into those equivalent to the monolayer or bilayer bands. The monolayerlike band exists only in odd-layered graphenes and gives a strong diamagnetic peak at $\varepsilon_F=0$. The bilayerlike bands al-

ways exist and present a strong diamagnetism in the vicinity of zero energy, unless the fine band structure caused by γ_3 is destroyed by the disorder.

ACKNOWLEDGMENTS

This work has been supported in part by the 21st Century COE Program at Tokyo Tech "Nanometer-Scale Quantum Physics" and by Grants-in-Aid for Scientific Research from the Ministry of Education, Culture, Sports, Science and Technology, Japan.

APPENDIX A: EFFECTIVE MASS HAMILTONIAN

We derive in the following the effective mass equation [Eq. (6)] describing states in the vicinity of K point in a multilayer graphene by starting from the one-orbital tight-binding model. The following is nothing but a straightforward extension of the monolayer case.[13,36] In a tight-binding model, the wave function is written as

$$\psi(\mathbf{r}) = \sum_j \left[\sum_{\mathbf{R}_{A_j}} \psi_{A_j}(\boldsymbol{\rho}_{A_j}) \phi(\mathbf{r} - \mathbf{R}_{A_j}) + \sum_{\mathbf{R}_{B_j}} \psi_{B_j}(\boldsymbol{\rho}_{B_j}) \phi(\mathbf{r} - \mathbf{R}_{B_j}) \right], \tag{A1}$$

where $j=1,2,\ldots,N$ is the layer index, and $\phi(\mathbf{r})$ is the wave function of the p_z orbital of a carbon atom located at the origin, as a function of three-dimensional position $\mathbf{r}$. $\mathbf{R}_X$ is the three-dimensional position of the site X, and $\boldsymbol{\rho}_X$ is a two-dimensional component of $\mathbf{R}_X$, parallel to the layer.

In the model including hopping parameters γ_0, γ_1, and γ_3 defined in Sec. II, Schrödinger's equation can be written as follows. For odd j,

$$\varepsilon \psi_{A_j}(\boldsymbol{\rho}_{A_j}) = -\gamma_0 \sum_{l=1}^{3} \psi_{B_j}(\boldsymbol{\rho}_{A_j} - \boldsymbol{\tau}_l) + \gamma_3 \sum_{l=1}^{3} [\psi_{B_{j+1}}(\boldsymbol{\rho}_{A_j} + \boldsymbol{\tau}_l) + \psi_{B_{j-1}}(\boldsymbol{\rho}_{A_j} + \boldsymbol{\tau}_l)], \tag{A2}$$

$$\varepsilon \psi_{B_j}(\boldsymbol{\rho}_{B_j}) = -\gamma_0 \sum_{l=1}^{3} \psi_{A_j}(\boldsymbol{\rho}_{B_j} + \boldsymbol{\tau}_l) + \gamma_1 [\psi_{A_{j+1}}(\boldsymbol{\rho}_{B_j}) + \psi_{A_{j-1}}(\boldsymbol{\rho}_{B_j})]. \tag{A3}$$

For even j,

$$\varepsilon \psi_{A_j}(\boldsymbol{\rho}_{A_j}) = -\gamma_0 \sum_{l=1}^{3} \psi_{B_j}(\boldsymbol{\rho}_{A_j} - \boldsymbol{\tau}_l) + \gamma_1 [\psi_{B_{j+1}}(\boldsymbol{\rho}_{A_j}) + \psi_{B_{j-1}}(\boldsymbol{\rho}_{A_j})], \tag{A4}$$

$$\varepsilon \psi_{B_j}(\boldsymbol{\rho}_{B_j}) = -\gamma_0 \sum_{l=1}^{3} \psi_{A_j}(\boldsymbol{\rho}_{B_j} + \boldsymbol{\tau}_l) + \gamma_3 \sum_{l=1}^{3} [\psi_{A_{j+1}}(\boldsymbol{\rho}_{B_j} - \boldsymbol{\tau}_l) + \psi_{A_{j-1}}(\boldsymbol{\rho}_{B_j} - \boldsymbol{\tau}_l)]. \tag{A5}$$

Here, we introduced the vectors from the B site to the nearest neighboring A sites as $\boldsymbol{\tau}_1 = a(0, 1/\sqrt{3})$, $\boldsymbol{\tau}_2 = a(-1/2, -1/2\sqrt{3})$, and $\boldsymbol{\tau}_3 = a(1/2, -1/2\sqrt{3})$, and we set $\psi_{A_0} = \psi_{B_0} = \psi_{A_{N+1}} = \psi_{B_{N+1}} = 0$.

The states around the K point can be expressed in terms of the slowly varying envelope functions F_{A_j}, F_{B_j} as

$$\psi_{A_j}(\boldsymbol{\rho}_{A_j}) = C_{A_j} e^{i\mathbf{K}\cdot\boldsymbol{\rho}_{A_j}} F_{A_j}(\boldsymbol{\rho}_{A_j}), \tag{A6}$$

$$\psi_{B_j}(\boldsymbol{\rho}_{B_j}) = C_{B_j} e^{i\mathbf{K}\cdot\boldsymbol{\rho}_{B_j}} F_{B_j}(\boldsymbol{\rho}_{B_j}), \tag{A7}$$

where $\mathbf{K} = (2\pi/a)(1/3, 1/\sqrt{3})$, and C_{A_j}, C_{B_j} are phase factors defined by

$$C_{A_j} = -\omega^{-1}, \quad C_{B_j} = 1 \quad (j \text{ odd}), \tag{A8}$$

$$C_{A_j} = 1, \quad C_{B_j} = -\omega \quad (j \text{ even}), \tag{A9}$$

with $\omega = \exp(2\pi i/3)$. When $\boldsymbol{\tau}_l$ is much smaller than the length scale of the envelope functions, we have

$$\psi_X(\boldsymbol{\rho} \pm \boldsymbol{\tau}_l) \approx e^{i\mathbf{K}\cdot(\boldsymbol{\rho}\pm\boldsymbol{\tau}_l)} \left(1 \pm \boldsymbol{\tau}_l \cdot \frac{\partial}{\partial \boldsymbol{\rho}}\right) F_X(\boldsymbol{\rho}), \tag{A10}$$

with $X = A_j$ or B_j.

By substituing Eq. (A7) with (A10) into Schrödinger's equations (A3) and (A5), we have for odd j,

$$\varepsilon F_{A_j}(\boldsymbol{\rho}) = \gamma k_- F_{B_j}(\boldsymbol{\rho}) + \gamma' k_+ [F_{B_{j-1}}(\boldsymbol{\rho}) + F_{B_{j+1}}(\boldsymbol{\rho})],$$

$$\varepsilon F_{B_j}(\boldsymbol{\rho}) = \gamma k_+ F_{A_j}(\boldsymbol{\rho}) + \gamma_1 [F_{A_{j-1}}(\boldsymbol{\rho}) + F_{A_{j+1}}(\boldsymbol{\rho})], \tag{A11}$$

and for even j,

$$\varepsilon F_{A_j}(\boldsymbol{\rho}) = \gamma k_- F_{B_j}(\boldsymbol{\rho}) + \gamma_1 [F_{B_{j-1}}(\boldsymbol{\rho}) + F_{B_{j+1}}(\boldsymbol{\rho})],$$

$$\varepsilon F_{B_j}(\boldsymbol{\rho}) = \gamma k_+ F_{A_j}(\boldsymbol{\rho}) + \gamma' k_- [F_{A_{j-1}}(\boldsymbol{\rho}) + F_{A_{j+1}}(\boldsymbol{\rho})], \tag{A12}$$

where $k_\pm = k_x \pm i k_y$ with $k_x = \frac{1}{i}\frac{\partial}{\partial x}$, $k_y = \frac{1}{i}\frac{\partial}{\partial y}$. We also used an identity

$$\sum_{l=1}^{3} e^{-i\mathbf{K}\cdot\boldsymbol{\tau}_l} (1 \quad \tau_l^x \quad \tau_l^y) = \frac{\sqrt{3}}{2} a\omega^{-1} (0 \quad i \quad 1). \tag{A13}$$

If we rewrite this set of equations into the matrix form for a vector $(F_{A_1}, F_{B_1}, F_{A_2}, F_{B_2}, \ldots)$, we finally obtain the Hamiltonian matrix [Eq. (6)]. The effective Hamiltonian for another valley $\mathbf{K}' = (2\pi/a)(2/3, 0)$ can be derived in a parallel way, while ω and ω^{-1} are exchanged in Eq. (A9).

APPENDIX B: SUSCEPTIBILITY FORMULA

The susceptibility formula [Eq. (30)] with [Eq. (31)] has been derived for the Luttinger-Kohn representation of the Bloch function[52] and therefore in systems described by the Hamiltonian consisting of the free electron kinetic energy $\hbar^2\hat{\mathbf{k}}^2/2m$ and terms linear in $\hat{\mathbf{k}}$.[44] We derive here the susceptibility formula which is valid in the general Hamiltonian $\mathcal{H}(\hat{\mathbf{k}})$, which includes k-square terms in off-diagonal matrix elements as well as k-linear terms. We shall confine ourselves to the case without electron-electron interaction for simplicity.

Consider the system described by the Schrödinger equation

$$\mathcal{H}\left[\hat{\mathbf{k}}+\frac{e}{\hbar}\mathbf{A}(\mathbf{r}),\mathbf{r}\right]\psi_\alpha(\mathbf{r})=\varepsilon_\alpha\psi_\alpha(\mathbf{r}), \tag{B1}$$

with $\hat{\mathbf{k}}=-i\nabla$ and $\mathbf{A}$ being the vector potential. The thermodynamic function Ω is given by

$$\begin{aligned}\Omega &= -k_BTg_s\frac{1}{V}\sum_\alpha \ln\{1+\exp[\beta(\mu-\varepsilon_\alpha)]\}\\ &= -k_BTg_s\frac{1}{V}\int d\varepsilon\left(-\frac{1}{\pi}\right)\mathrm{Im\ Tr}\frac{1}{\varepsilon-\mathcal{H}+i0}\\ &\quad\times\ln\{1+\exp[\beta(\mu-\varepsilon)]\},\end{aligned} \tag{B2}$$

where g_s is the spin degeneracy and V is the system volume.

We consider an isotropic system and assume the vector potential $\mathbf{A}=(0,A)$, with

$$A(x)=\frac{B}{2iq}(e^{iqx}-e^{-iqx}),\quad B(x)=B\cos(qx), \tag{B3}$$

where we are going to take the long wavelength limit $q\to 0$, for which the field causes the response the same as that due to a spatially uniform magnetic field. In the presence of this vector potential, the Hamiltonian changes from $\mathcal{H}(\hat{\mathbf{k}})$ to $\mathcal{H}(\hat{\mathbf{k}}+\Delta\mathbf{k})$, with $\Delta\mathbf{k}=(0,\Delta k)$, where $\Delta k=(e/\hbar)A(x)$. The Hamiltonian can be expanded as

$$\mathcal{H}(\hat{\mathbf{k}}+\Delta\mathbf{k})=\mathcal{H}_0+\frac{1}{2}(\Delta k\mathcal{H}_y+\mathcal{H}_y\Delta k)+\frac{1}{2}(\Delta k)^2\mathcal{H}_{yy}, \tag{B4}$$

where $\mathcal{H}_0\equiv\mathcal{H}(\mathbf{k})$, $\mathcal{H}_y\equiv\partial\mathcal{H}_0/\partial\hat{k}_y$, and $\mathcal{H}_{yy}\equiv\partial^2\mathcal{H}_0/\partial\hat{k}_y^2$. Note that, in general, k-square Hamiltonian Δk does not commute with $\mathcal{H}_y$ but does with $\mathcal{H}_{yy}$.

Expanding the Hamiltonian up to the second order in the strength of the magnetic field B, we have

$$\begin{aligned}\mathrm{Tr}\left(\frac{1}{\varepsilon-\mathcal{H}}-\frac{1}{\varepsilon-\mathcal{H}_0}\right) &= \frac{1}{(2iql^2)^2}\frac{\partial}{\partial\varepsilon}\mathrm{Tr}\left(\frac{1}{\varepsilon-\mathcal{H}_0}\mathcal{H}_{yy}\right.\\ &\quad\left.+\frac{1}{\varepsilon-\mathcal{H}_{\mathbf{q}/2}}\mathcal{H}_y\frac{1}{\varepsilon-\mathcal{H}_{-\mathbf{q}/2}}\mathcal{H}_y\right),\end{aligned} \tag{B5}$$

where $l=\sqrt{\hbar/eB}$ is the magnetic length, $\mathcal{H}_\mathbf{q}=\mathcal{H}(\hat{\mathbf{k}}+\mathbf{q})$, $\mathbf{q}=(q,0)$, and we assumed that the system is translational invariant (after the configuration average in the presence of impurities).

We then expand $\mathcal{H}_\mathbf{q}$ up to the second order in q to have

$$\begin{aligned}\mathrm{Tr}\left(\frac{1}{\varepsilon-\mathcal{H}}-\frac{1}{\varepsilon-\mathcal{H}_0}\right) &= \frac{1}{16l^4}\frac{\partial}{\partial\varepsilon}\mathrm{Tr}\left(G\mathcal{H}_xG\mathcal{H}_yG\mathcal{H}_xG\mathcal{H}_y\right.\\ &\quad-2G\mathcal{H}_xG\mathcal{H}_xG\mathcal{H}_yG\mathcal{H}_y\\ &\quad-\frac{1}{2}G\mathcal{H}_yG\mathcal{H}_{xx}G\mathcal{H}_y\\ &\quad\left.-\frac{1}{2}G\mathcal{H}_xG\mathcal{H}_{yy}G\mathcal{H}_x\right),\end{aligned} \tag{B6}$$

with $G=(\varepsilon-\mathcal{H}_0)^{-1}$. This immediately gives the change of the thermodynamic potential $\Delta\Omega=\Omega(B)-\Omega(0)$ with Eq. (B2). The susceptibility χ is obtained by a relation $\Delta\Omega=-(1/2)\chi\langle B(x)^2\rangle=(1/4)\chi B^2$ as

$$\begin{aligned}\chi &= \frac{g_s}{4V}\frac{e^2}{\hbar^2}\int d\varepsilon f(\varepsilon)\left(-\frac{1}{\pi}\right)\mathrm{Im\ Tr}\left(G\mathcal{H}_xG\mathcal{H}_yG\mathcal{H}_xG\mathcal{H}_y\right.\\ &\quad-2G\mathcal{H}_xG\mathcal{H}_xG\mathcal{H}_yG\mathcal{H}_y-\frac{1}{2}G\mathcal{H}_yG\mathcal{H}_{xx}G\mathcal{H}_y\\ &\quad\left.-\frac{1}{2}G\mathcal{H}_xG\mathcal{H}_{yy}G\mathcal{H}_x\right).\end{aligned} \tag{B7}$$

This gives Eq. (30) with Eq. (61) for the multilayer graphene.

When Δk commutes with $\mathcal{H}_y$, we can simplify the formula by noting in Eq. (B5) that

$$\begin{aligned}\mathrm{Tr}\left(\frac{1}{\varepsilon-\mathcal{H}_{\mathbf{q}/2}}\mathcal{H}_y\frac{1}{\varepsilon-\mathcal{H}_{-\mathbf{q}/2}}\mathcal{H}_y\right) &= \mathrm{Tr}\left(\frac{1}{\varepsilon-\mathcal{H}_\mathbf{q}}\mathcal{H}_y\frac{1}{\varepsilon-\mathcal{H}_0}\mathcal{H}_y\right)\\ &= \mathrm{Tr}\left(\frac{1}{\varepsilon-\mathcal{H}_0}\mathcal{H}_y\frac{1}{\varepsilon-\mathcal{H}_{-\mathbf{q}}}\mathcal{H}_y\right).\end{aligned} \tag{B8}$$

The susceptibility becomes

$$\chi=\frac{g_s}{2V}\frac{e^2}{\hbar^2}\int d\varepsilon f(\varepsilon)\left(-\frac{1}{\pi}\right)\mathrm{Im\ Tr}(G\mathcal{H}_xG\mathcal{H}_yG\mathcal{H}_xG\mathcal{H}_y), \tag{B9}$$

giving Eq. (30) with Eq. (31).

[1] K. S. Novoselov, A. K. Geim, S. V. Morozov, D. Jiang, Y. Zhang, S. V. Dubonos, I. V. Grigorieva, and A. A. Firsov, Science **306**, 666 (2004).
[2] K. S. Novoselov, A. K. Geim, S. V. Morozov, D. Jiang, M. I. Katsnelson, I. V. Grigorieva, S. V. Dubonos, and A. A. Firsov, Nature (London) **438**, 197 (2005).
[3] Y. Zhang, Y. W. Tan, H. L. Stormer, and P. Kim, Nature (London) **438**, 201 (2005).
[4] J. W. McClure, Phys. Rev. **104**, 666 (1956).
[5] D. P. DiVincenzo and E. J. Mele, Phys. Rev. B **29**, 1685 (1984).
[6] J. Gonzalez, F. Guinea, and M. A. H. Vozmediano, Nucl. Phys. B **424**, 595 (1994).
[7] J. Gonzalez, F. Guinea, and M. A. H. Vozmediano, Phys. Rev. Lett. **77**, 3589 (1996).

[8] N. H. Shon and T. Ando, J. Phys. Soc. Jpn. **67**, 2421 (1998).
[9] J. Gonzalez, F. Guinea, and M. A. H. Vozmediano, Phys. Rev. B **63**, 134421 (2001).
[10] Y. Zheng and T. Ando, Phys. Rev. B **65**, 245420 (2002).
[11] T. Ando, Y. Zheng, and H. Suzuura, J. Phys. Soc. Jpn. **71**, 1318 (2002).
[12] H. Suzuura and T. Ando, Phys. Rev. Lett. **89**, 266603 (2002).
[13] T. Ando, J. Phys. Soc. Jpn. **74**, 777 (2005).
[14] K. S. Novoselov, E. McCann, S. V. Morozov, V. I. Falko, M. I. Katsnelson, U. Zeitler, D. Jiang, F. Schedin, and A. K. Geim, Nat. Phys. **2**, 177 (2006).
[15] T. Ohta, A. Bostwick, T. Seyller, K. Horn, and E. Rotenberg, Science **313**, 951 (2006); T. Ohta, A. Bostwick, J. L. McChesney, T. Seyller, K. Horn, and E. Rotenberg, Phys. Rev. Lett. **98**, 206802 (2007).
[16] E. McCann and V. I. Fal'ko, Phys. Rev. Lett. **96**, 086805 (2006).
[17] E. McCann, Phys. Rev. B **74**, 161403(R) (2006).
[18] M. Koshino and T. Ando, Phys. Rev. B **73**, 245403 (2006).
[19] J. Nilsson, A. H. Castro Neto, F. Guinea, and N. M. R. Peres, Phys. Rev. Lett. **97**, 266801 (2006).
[20] J. Nilsson and A. H. Castro Neto, Phys. Rev. Lett. **98**, 126801 (2007).
[21] F. Guinea, A. H. Castro Neto, and N. M. R. Peres, Phys. Rev. B **73**, 245426 (2006).
[22] S. Latil and L. Henrard, Phys. Rev. Lett. **97**, 036803 (2006).
[23] B. Partoens and F. M. Peeters, Phys. Rev. B **74**, 075404 (2006).
[24] C. L. Lu, C. P. Chang, Y. C. Huang, J. M. Lu, C. C. Hwang, and M. F. Lin, J. Phys.: Condens. Matter **18**, 5849 (2006).
[25] J. W. McClure, Phys. Rev. **108**, 612 (1957); **119**, 606 (1960).
[26] M. P. Sharma, L. G. Johnson, and J. W. McClure, Phys. Rev. B **9**, 2467 (1974).
[27] S. A. Safran and F. J. DiSalvo, Phys. Rev. B **20**, 4889 (1979).
[28] S. A. Safran, Phys. Rev. B **30**, 421 (1984).
[29] R. Saito and H. Kamimura, Phys. Rev. B **33**, 7218 (1986).
[30] S. G. Sharapov, V. P. Gusynin, and H. Beck, Phys. Rev. B **69**, 075104 (2004).
[31] H. Fukuyama, J. Phys. Soc. Jpn. **76**, 043711 (2007).
[32] M. Koshino and T. Ando, Phys. Rev. B **75**, 235333 (2007).
[33] P. R. Wallace, Phys. Rev. **71**, 622 (1947).
[34] J. C. Slonczewski and P. R. Weiss, Phys. Rev. **109**, 272 (1958).
[35] G. Dresselhaus and M. S. Dresselhaus, Phys. Rev. **140**, A401 (1965).
[36] H. Ajiki and T. Ando, J. Phys. Soc. Jpn. **62**, 1255 (1993).
[37] C. L. Kane and E. J. Mele, Phys. Rev. Lett. **78**, 1932 (1997).
[38] J.-C. Charlier, X. Gonze, and J.-P. Michenaud, Phys. Rev. B **43**, 4579 (1991).
[39] W. W. Toy, M. S. Dresselhaus, and G. Dresselhaus, Phys. Rev. B **15**, 4077 (1977).
[40] A. Misu, E. Mendez, and M. S. Dresselhaus, J. Phys. Soc. Jpn. **47**, 199 (1979).
[41] R. E. Doezema, W. R. Datars, H. Schaber, and A. Van Schyndel, Phys. Rev. B **19**, 4224 (1979).
[42] E. V. Castro, K. S. Novoselov, S. V. Morozov, N. M. R. Peres, J. M. B. Lopes dos Santos, J. Nilsson, F. Guinea, A. K. Geim, and A. H. Castro Neto, arXiv:cond-mat/0611342.
[43] T. Ohno and H. Kamimura, J. Phys. Soc. Jpn. **52**, 223 (1983).
[44] H. Fukuyama, Prog. Theor. Phys. **45**, 704 (1971).
[45] H. Fukuyama and R. Kubo, J. Phys. Soc. Jpn. **28**, 570 (1970).
[46] M. Nakamura, arXiv:cond-mat/0703355.
[47] H. L. Stormer, T. Haavasoja, V. Narayanamurti, A. C. Gossard, and W. Wiegmann, J. Vac. Sci. Technol. B **1**, 423 (1983).
[48] I. Meinel, D. Grundler, S. Bargstädt-Franke, C. Heyn, and D. Heitmann, Appl. Phys. Lett. **70**, 3305 (1997).
[49] J. P. Eisenstein, H. L. Stormer, V. Narayanamurti, A. Y. Cho, A. C. Gossard, and C. W. Tu, Phys. Rev. Lett. **55**, 875 (1985).
[50] A. Potts, R. Shepherd, W. G. Herrenden-Harker, M. Elliott, C. L. Jones, A. Usher, G. A. C. Jones, D. A. Ritchie, E. H. Linfield, and M. Grimshaw, J. Phys.: Condens. Matter **8**, 5189 (1996).
[51] S. A. J. Wiegers, M. Specht, L. P. Levy, M. Y. Simmons, D. A. Ritchie, A. Cavanna, B. Etienne, G. Martinez, and P. Wyder, Phys. Rev. Lett. **79**, 3238 (1997).
[52] J. M. Luttinger and W. Kohn, Phys. Rev. **97**, 869 (1955).